electronics

Article

A Wireless Data Transfer by Using a Patch Antenna for Biomedical Applications

Gyung-Su Byun

School of Information and Communication Engineering, Inha University, Incheon 22212, Republic of Korea; gsbyun@inha.ac.kr

Abstract: In this paper, a 20 GHz wireless data transfer (WDT) interface for implantable applications is proposed. The proposed WDT utilizes a small-form factor off-chip antenna to transfer data through a human body. By using the implantable antenna, the biomedical WDT system occupies a smaller chip size, which is suitable for future biomedical applications. The proposed WDT system with a small-form factor patch antenna and near-threshold VCO operates at 20 GHz, has a data rate of 1.8 Gb/s and consumes only a low power of 5.4 pJ/b.

Keywords: wireless data transfer (WDT); bio-medical antenna; patch antenna

1. Introduction

Biomedical implants such as wireless brain sensors [1] can greatly improve the quality of healthcare for the continuous monitoring of vital signs. Advances in semiconductor technology have helped to improve the key performance of biomedical applications [2–6]. The most important challenge in future implantable medical devices (IMDs) is to provide a power-efficient small-form factor and higher bandwidth. The most important factor is to design a high-sensitivity antenna and a high-performance wireless data transfer (WDT) microsystem. Conventional IMDs typically use frequency bands such as the medical implant communications service (MICS) band (i.e., 400 MHz) and the industrial, scientific and medical (ISM) bands (i.e., 900 MHz, 2.4 GHz and 4.8 GHz) [7]. However, those traditional implantable antennas have a large footprint and a low gain value due to the low operation frequency. Furthermore, RF transceivers for biomedical devices have a higher power consumption. For example, the high-performance oscillator usually consumes high power for RF carrier (de)-modulation and carrier synchronization [8]. In recent years, the operating frequency of biomedical antennas and WDT systems exceeded the aforementioned MICS and ISM bands (i.e., 10 GHz [9,10], 15 GHz [11], 22 GHz [12] and 94 GHz [13]) for versatile biomedical applications such as skin or implantable cancer detection. Therefore, designing small-form factor implantable antennas and ultra-low-power WDT transceivers is the most important design factor. However, there are the key trade-offs between the antenna geometry (i.e., size) and radiation efficiency when the antenna size gets smaller and smaller. In this paper, we proposed a high-performance and small-form factor biomedical patch antenna by utilizing two combinations of notches and slots to improve the surface current distribution and radiation efficiency significantly. In addition, the proposed biomedical WDT system is also analyzed and designed by incorporating an ultra-low-power oscillator which operates at a near-threshold voltage (NTV) to reduce the power consumption of the overall system. The proposed antenna works at 20 GHz with a smaller size (i.e., 15.9 mm^2) and a higher antenna gain (5.5 dBi). The WDT system has an improved power efficiency (i.e., 5.4 pJ/b.)

Figure 1 shows the block diagram of a general wireless biomedical microsystem. The neural data inside the body can be communicated by a neural link which is composed of a spike detector, sampled by an ADC and fed into a digital signal processing (DSP) unit and RF transceiver for wireless data and power transfer systems [3]. The neural

Citation: Byun, G.-S. A Wireless Data Transfer by Using a Patch Antenna for Biomedical Applications. *Electronics* **2022**, *11*, 4197. https://doi.org/10.3390/electronics11244197

Academic Editors: Andrea Boni and Michele Caselli

Received: 29 June 2022
Accepted: 17 October 2022
Published: 15 December 2022

data can be transceived by the RF transmitter (RFTX), receiver (RFRX) and biomedical antenna. The RFTX can amplify the neural signal and modulate the signal into an RF carrier, and the implantable antenna can transmit the carrier signal wirelessly. The RFRX can act as an envelope detector to de-modulate the modulated RF carrier signal to a baseband original signal [14]. The most important factors in bio-telemetry systems are the energy efficiency and small-form factor. Our proposed bio-telemetry system including a biomedical antenna utilizes a VCO using near-threshold supply voltage to reduce power consumption significantly and also uses a bio-compatible compact patch or loop antenna for robust biomedical data communication.

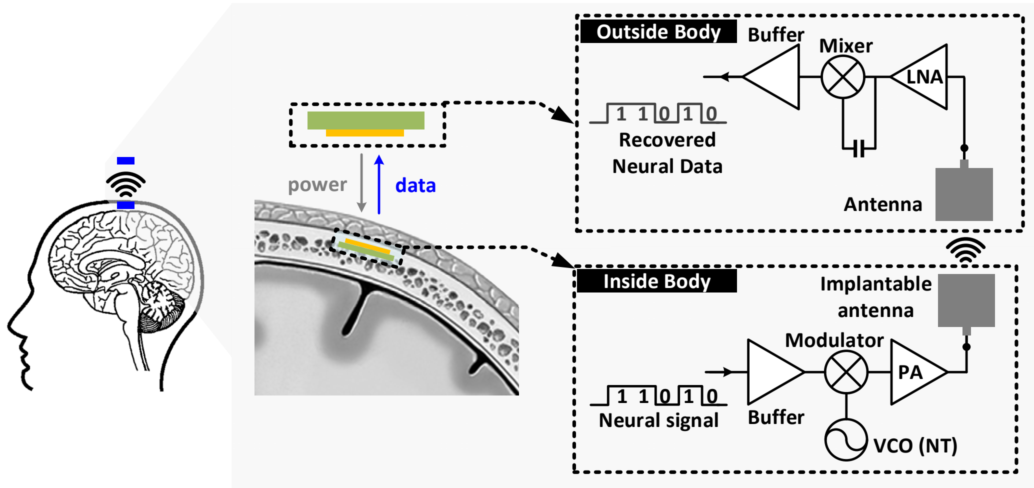

Figure 1. A wireless data link between a patch antenna for biomedical applications.

2. Biomedical Patch Antenna

2.1. Proposed Implantable Notch Antenna Design

Figure 2 shows the block diagram of the proposed biomedical compact patch antenna with slots. The proposed biomedical antenna consists of a square patch with an inset-feed line with an FR4 substrate. The most important factor of a patch antenna has advantages such as its (1) light weight, (2) low cost, (3) enhanced flexibility of polarization, (4) easy implementation of multi-band operation and (5) easy integration with microwave circuits. The patch antenna is composed of a 7.6 mm-wide ground plane with a 0.5 mm-thick substrate layer and is also fed by a 50 Ohm inset-fed line. The radiation efficiency can be optimized by the key parameters of antenna geometry; Wp, Lp and Wf are the width, the length of the patch and the feed line width, respectively. Ws and Ls are slot width and slot length, respectively. To design the optimal antenna with a wider bandwidth and enhanced radiation efficiency, the width, length and slot shapes are analyzed and verified.

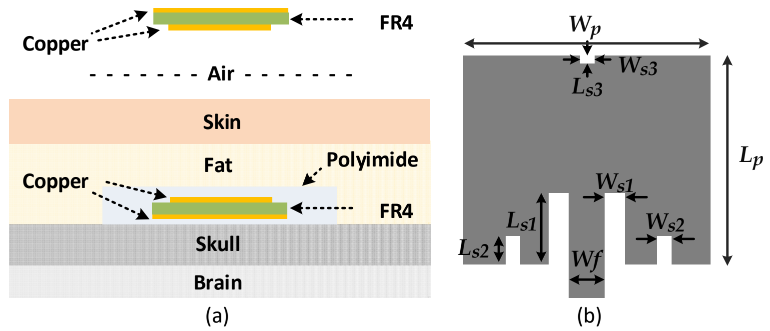

Parameter	*Dimension*
Lp	*3.48 mm*
Wp	*4.56 mm*
Ls1	*1.1 mm*
Ws1	*0.175 mm*
Ls2	*0.5 mm*
Ws2	*0.1 mm*
Ls3	*0.1 mm*
Ws3	*0.1 mm*
Wf	*0.95 mm*

(c)

Figure 2. Proposed patch antenna model. (**a**) Cross-section of the layer structure, (**b**) proposed patch antenna with notches and (**c**) antenna design parameters.

2.2. Patch Antenna Optimization

Figure 3 shows the structure of a typical patch antenna and a patch antenna with notches and slots for high-gain operation. The slot size variables can change the effective patch antenna size and also improve the target resonance frequency characteristics [15]. The proposed antenna design with optimal slot shapes is applied to acquire a scalp-implantable patch antenna at 20 GHz. The optimized antenna with slots can further be adjusted in terms of slot length (or width) in order to overcome this effect while preserving excellent impedance matching characteristics.

Figure 3. Geometries of the patch antenna for high-gain operation. (**a**) Common patch antenna, (**b**) patch antenna with an improved notch and slot structure.

Figure 4 shows the optimal return loss with the patch antenna with the desired resonant frequencies. The optimal patch antenna can achieve a return loss below −40 dB, and the simulated −10 dB bandwidth at 20 GHz is 940 MHz. The miniaturized feed line is also further optimized to provide good impedance matching characteristics and achieve a small-form factor.

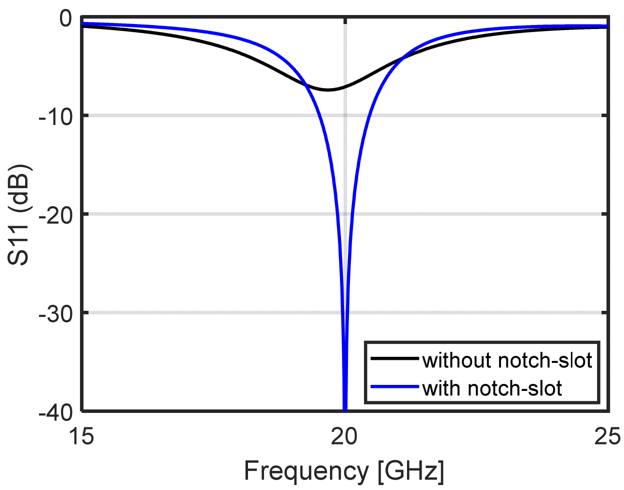

Figure 4. Simulated S_{11} frequency characteristics with notch slot antenna.

The proposed antennas with the optimal slot geometry exhibit bandwidths (defined at −10 dB) of approximately 940 MHz and also show improved far-field gain radiation patterns, as shown in Figure 5. For example, our proposed antenna with and without notches provides 5.5 dB and 4.7 dB, respectively. The proposed notch-based antenna structure can provide a much higher radiation gain efficiency (17% higher with the notch-based antenna).

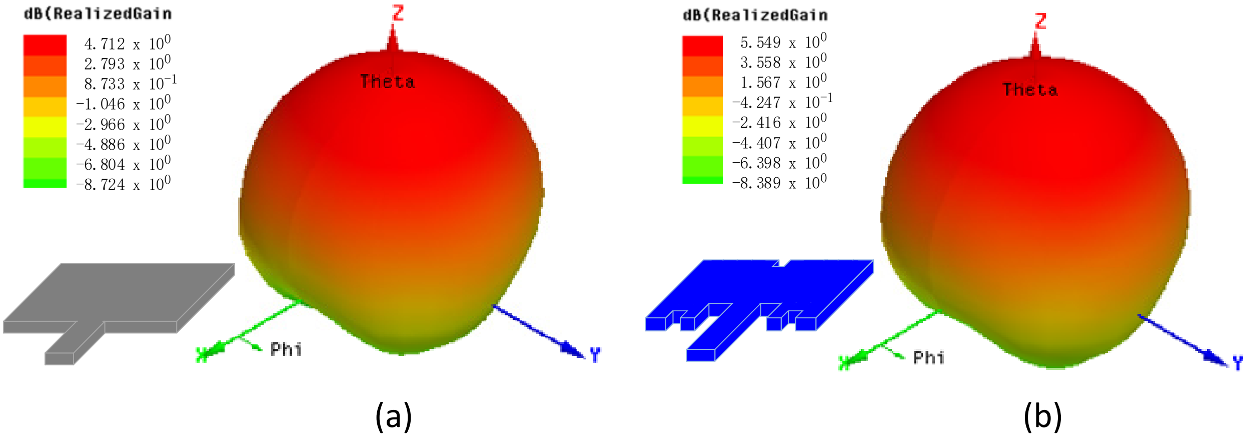

Figure 5. 3D far-field gain radiation patterns: (**a**) without a notch-slot, (**b**) with a notch-slot antenna.

Figure 6 shows the surface current distribution of different biomedical patch antennas using a 3D EM simulator (i.e., HFSS). As shown in Figure 6b, the surface current density can be significantly enhanced by using the proposed notch-antenna at a 20 GHz operation frequency. The hybrid combination of two different notch patterns for the proposed antenna can further increase the surface current distribution and improve the antenna radiation efficiency [16]. Because the dielectric properties between the outside (i.e., air) and inside body could be different, the antenna outside the body has more design flexibility and notch-based geometry in order to increase the surface current redistribution and improve the antenna radiation efficiency.

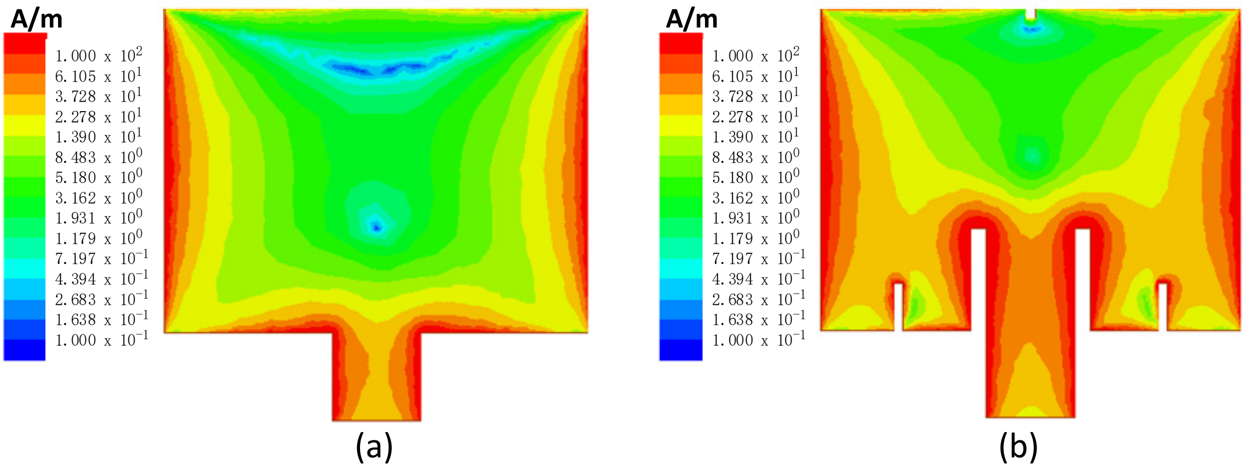

Figure 6. Simulated surface current distribution of the proposed patch antenna at 20 GHz: (**a**) without a notch-slot, (**b**) with a notch-slot antenna to increase the surface current distribution and antenna efficiency.

2.3. *Performance of the Proposed Notch-Based Patch Antenna*

Figure 7 shows the antenna configuration for a wireless biotelemetry system with a 10 mm air gap and E-field distribution of the antenna inside the body. The power pattern can be changed because the power pattern depends on the deflections and variation of the power distribution caused by the different depths of biomedical layers and the heterogeneous combination of biomedical layers [17]. Table 1 provides the dielectric properties of the human brain and other biomedical layers at higher frequencies because the absorption ratio and EM radiation pattern can be slightly affected depending on higher operation frequencies [12,13,18,19].

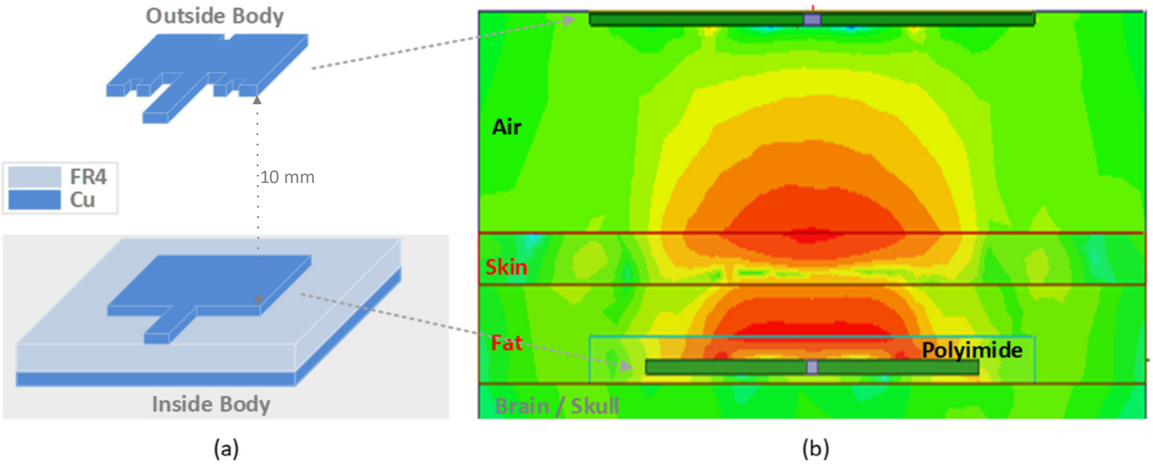

Figure 7. (**a**) WDT's antenna with a 10 mm air gap and (**b**) E-field distribution of the antenna.

Table 1. Dielectric properties of human tissue at higher frequencies [12,13,18,19].

Layer	Skin	Fat	Skull	Brain
ε_r	33.04	9.35	8.12	31.8
Δ (S/m)	6.27	1.32	2.14	10
Thickness (mm)	0.5	1	8	4

Figure 8 shows the 3D EM HFSS modeling with the spherical human head models and implantable patch antennas. To enhance the accuracy of the radiation pattern analysis, the accurate parameters of biomedical layers such as the dielectric constant (ε_r) and conductivity (δ) at higher frequencies are derived from the prior works [12,13,18,19].

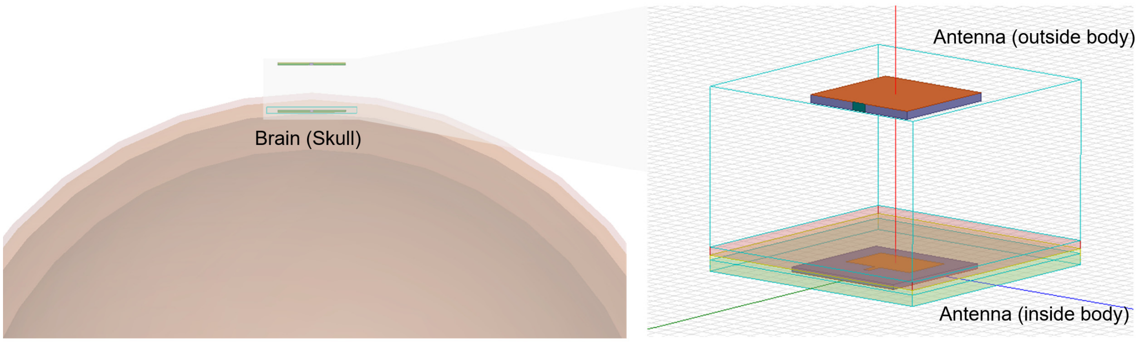

Figure 8. 3D EM HFSS modeling with the spherical human head models and patch antennas.

The air gap might influence the power gain of the antenna [20]. Typically, the air gap of a biomedical WDT system is 10 mm. However, the different air gap that is 10~30 mm was modeled and analyzed to verify the proposed WDT transceiver. For example, the air gap that is 30 mm has a severe power loss (i.e., −27 dB at 20 GHz). However, the low-noise amplifier (LNA) with a higher gain can easily recover the weakened signal. Figure 9 shows the result of simulated S21 frequency characteristics at different antenna gap distances. The loss of S21 is different at different antenna gap widths, but the center frequency is maintained. Therefore, the weakened neural signal through the wireless channel can be reconstructed using the proposed WDT transceiver capable of amplifying the signal waveform.

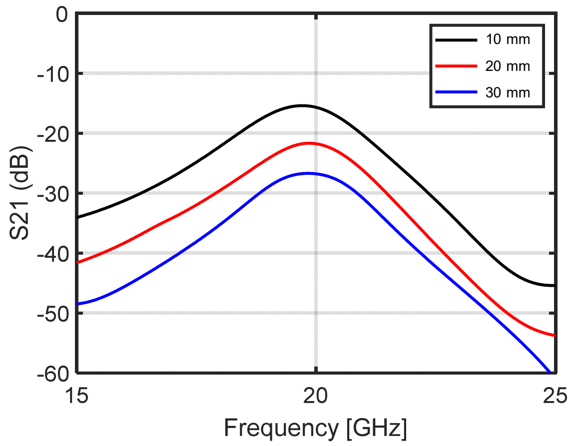

Figure 9. Effect of simulated S21 at different antenna gap distances with 10~30 mm.

Table 2 provides a comparison between the previously implantable CP antennas and the proposed antenna. The results show that our patch antenna has a smaller size and a wider bandwidth using a higher frequency than the others. Moreover, it is certain that, regardless of frequency, miniaturized size or return loss, our antenna has the advantage of a higher antenna gain among the published implantable antennas at the targeted resonance bands.

Table 2. Performance comparison of the implantable antennas.

Parameter	AWPL 2018 [20]	TAP 2019 [21]	TAP 2020 [22]	TAP 2020 [23]	TAP 2021 [24]	AWPL 2018 [25]	ACS 2021 [19]	This Work
Frequency (GHz)	0.9	0.9	2.4	2.4	2.4	4.8	22	20
Dimension (mm^2)	66.5	49	96	272.2	12	53.2	0.55	17
S11 (dB)	−30	−18	−26	−22	NA	−10	−19	−16
S11 ≤ -10dB (MHz)	112	107.5	540	140	525	115	NA	940
Gain (dBi)	−32.8	−27.65	−33	−11.3	−25.9	−12	−20	−0.07

3. Wireless Data Transfer (WDT) System for Biomedical Applications

3.1. Proposed WDT Transmitter Design

Figure 10 shows the proposed architecture of a wireless data transfer (WDT) transceiver for compact biotelemetry devices. A near-threshold voltage (NTV)-based oscillator is utilized to generate the desired differential LO for driving a modulator for a transmitter side.

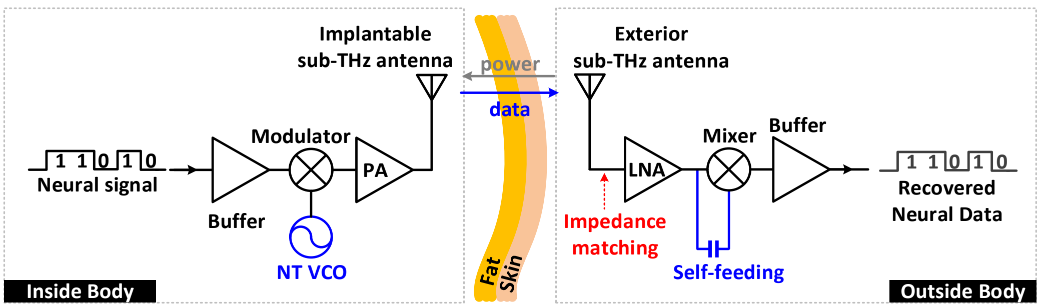

Figure 10. Proposed architecture of the WDT transceiver for biomedical applications.

The total power consumption of the NTV oscillator can be reduced significantly from 6.9 mW to 1.6 mW (i.e., almost four times lower power). Furthermore, the supply voltage of the NTV oscillator is 0.6 V, which provides better voltage headroom for the next-stage modulator and enhances the signal integrity of the transmitter. The power amplifier (PA) is designed using a class AB amplifier with a 50 Ω impedance feeding transmission line between the PA and the patch antenna for better signal integrity. The differential mutual mixer was utilized to down-convert the modulated carrier signal. Finally, an output buffer amplifies the mixer output.

Figure 11 shows the WDT transmitter and critical signal waveforms at each stage. The RF-band transmitter (RFTX) is composed of an input buffer, an LC tank VCO, a modulator and a power amplifier (PA). The LC-VCO uses a near-threshold supply to reduce the power consumption of the RFTX significantly. In the RFTX, the VCO first generates a local oscillator (LO) signal at 20 GHz, and the modulator up-converts by mixing the LO signal and the data input signal for ASK communication. A PA delivers an RF-modulated signal into a patch antenna for a higher power conversion [26].

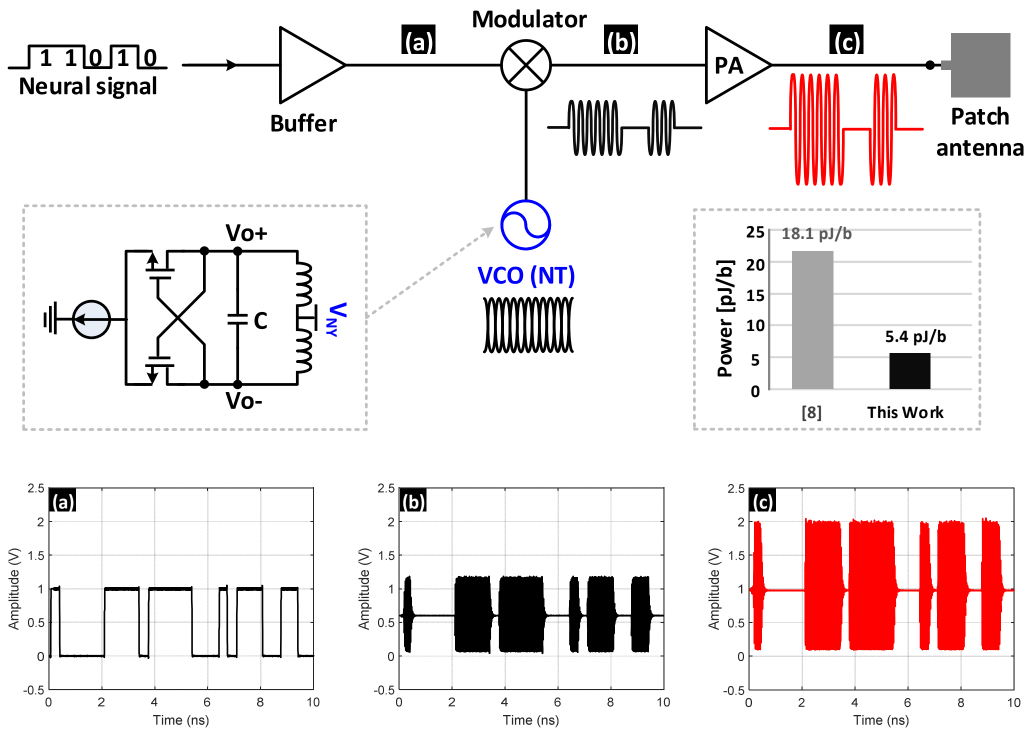

Figure 11. Simulated waveforms of the WDT TX using ASK modulation with the proposed NTVCO. (**a**) The output signal of the input-buffer, (**b**) the output signal of the modulation and (**c**) the output signal of the WDT TX.

3.2. Proposed WDT Receiver Design

Figure 12 shows the WDT receiver with a patch antenna and critical signal waveforms at each stage. The RF-band receiver (RFRX) demodulator uses a non-coherent direct down-conversion scheme to reduce the power consumption of the receiver significantly. The RFRX is composed of an LNA, a band-selective transformer, a self-feeding mixer and an output buffer. The LNA utilizes a CS stage configuration which integrates an inductive load to sustain a smaller DC voltage drop than a passive element [27]. Because the inductor can provide LC resonance with a loading and coupling capacitance, higher frequency operation can be better than a simple resistively loaded LNA. Furthermore, the LNA has another input inductor for a robust input-matching network [28]. This enhances the gain of the LNA because of the minimization of the signal loss of the RF-modulated carrier. At the next stage, a highly band-selective on-chip transformer is utilized to obtain an enhanced voltage gain through a higher coupling factor of k between the primary and secondary coil with an optimal turn ratio. Therefore, optimal n and k is the most important factor to design an on-chip transformer. A differential mutual-mixer which is composed of a self-mixer and a resistor-feedback amplifier down-converted the RF carrier signal into the baseband data D1 (RF). An output driver amplifies the recovered original BB data signal.

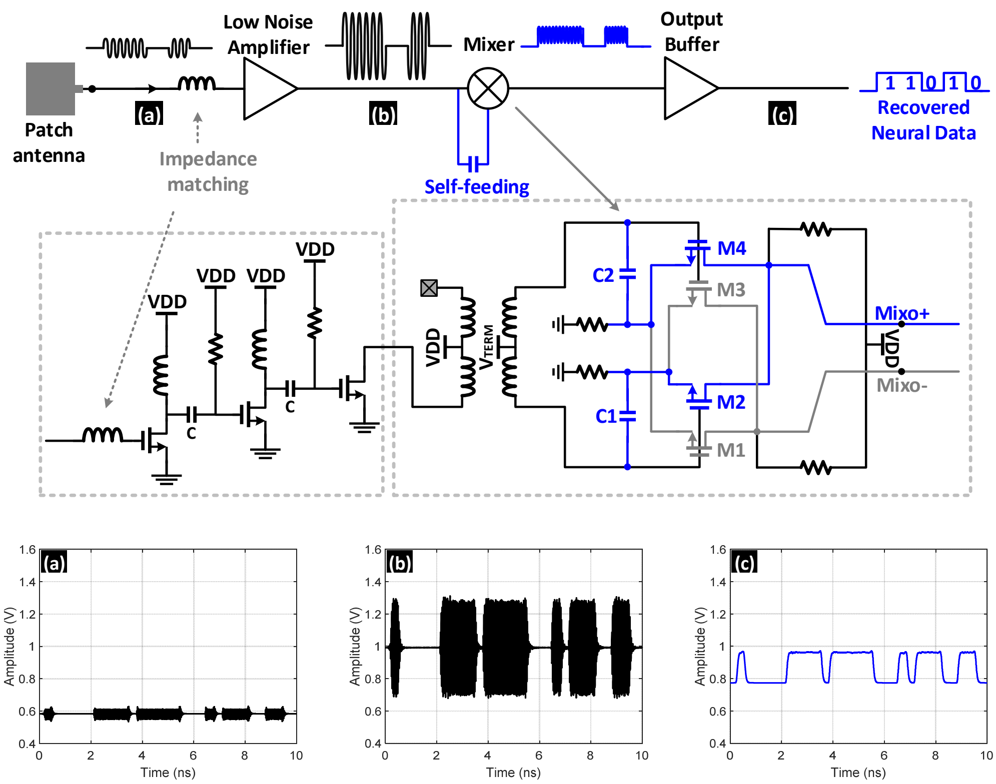

Figure 12. Simulated waveforms of the WDT RX with the proposed patch antenna. (**a**) The carrier signal of the patch antenna, (**b**) the output signal of the LNA and (**c**) the recovered output signal.

Figure 13 shows the layout of the WDT transmitter (TX) and receiver (RX). The proposed WDT circuits have been implemented in 28 nm CMOS technology. The chip sizes of the WDT transmitter and receiver are 0.038 mm^2 and 0.198 mm^2, respectively.

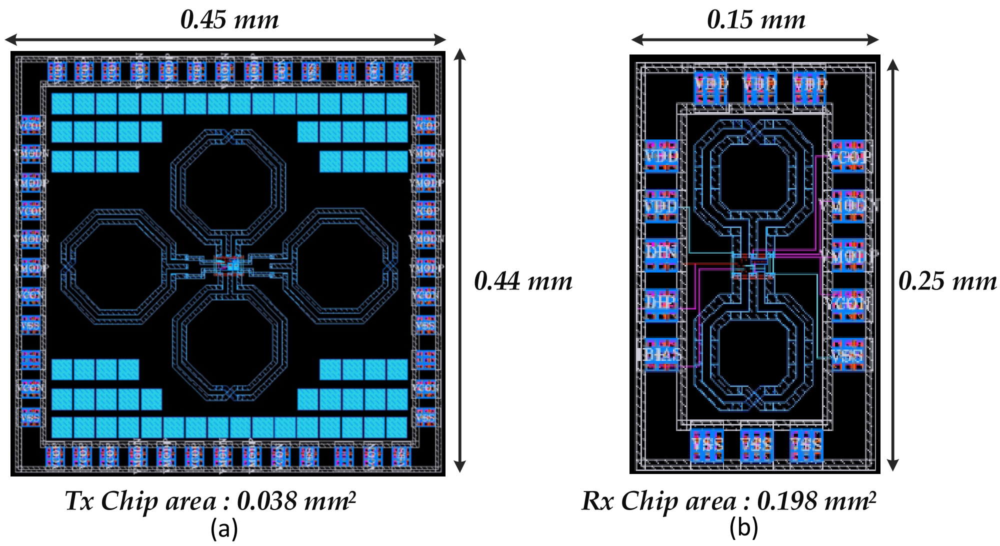

Figure 13. (**a**) Layout of the WDT TX, (**b**) layout of the WDT RX.

3.3. Performance Results of the Proposed WDT System

Figure 14 shows the Monte Carlo simulation results of the proposed WDT system. The simulation is performed to evaluate the high-volume manufacturing (HVM) mismatch's impact on our WDT by taking the process, temperature and voltage (PVT) variation into consideration. The main performance, such as the power efficiency and LNA input swing, is investigated. The PVT variation's impact on the key performance of the power efficiency (i.e., 112.17 uW = 37.39 uW × 3 @ 3σ) and LNA input swing (i.e., 29.88 mV = 9.96 mV × 3 @ 3σ) could be negligible.

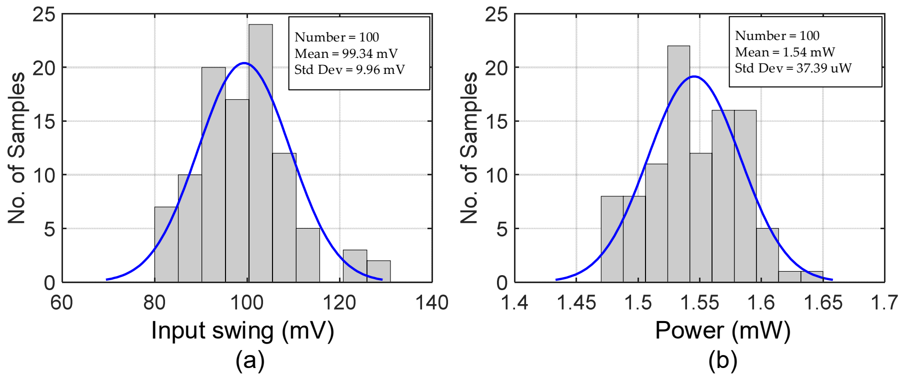

Figure 14. The Monte Carlo simulation results. (**a**) LNA input swing of the WDT, and (**b**) VCO Power mismatch.

Table 3 shows the performance comparison of the proposed WDT system with prior works [19–22,29]. The proposed WDT interface utilizing an NTV VCO scheme could provide a much higher power efficiency (i.e., 5.4 pJ/b) and data throughput (i.e., 1.8 Gb/s) to biotelemetry systems.

Table 3. Performance comparison of the proposed wireless data transfer.

Parameter	TICAS-II 2018 [30]	TICAS-I 2018 [31]	MWCL 2018 [32]	JETCAS 2018 [33]	TMTT 2020 [34]	JSSC 2017 [35]	This Work
CMOS technology	180 nm	130 nm	65 nm	65 nm	65 nm	28 nm	28 nm
Modulation	OOK	OOK	OOK	OOK	OOK	OOK	OOK
Freq. band (GHz)	6	4.5	4.1	8	60	4.5	20
Data rate (Mb/s)	200	1000	200	10	12.5	27.24	1800
Power supply (V)	1.8	1.2	1	1.2	NA	0.55	1
Energy (pJ/b)	20	5	4.3	21.6	2.65	14	5.4

4. Conclusions

A wireless data transfer (WDT) system with a biomedical patch antenna is proposed. The proposed WDT system with a notch-based biomedical patch antenna and near-threshold VCO operates at 20 GHz. By integrating the high-performance antenna with the notch and slot patterns to enhance the surface current distribution of the patch antenna, a broader bandwidth radiation pattern can be implemented, and by using the NTV oscillator, the power consumption can be reduced significantly. By utilizing the implantable antenna with 20 GHz, the WDT interface occupies a smaller chip size which is suitable for future biotelemetry system applications and enables a promising solution for future implantable devices.

Funding: This work was supported by the Inha University Research Grant under Grant INHA-00000. The EDA tool and design kit were helped by the IC Design Education Center(IDEC), Korea.

Institutional Review Board Statement: Not applicable.

Informed Consent Statement: Not applicable.

Conflicts of Interest: The authors declare no conflict of interest.

References

1. Poon, C.C.Y.; Lo, B.P.L.; Yuce, M.R.; Alomainy, A.; Hao, Y. Body Sensor Networks: In the Era of Big Data and Beyond. *IEEE Rev. Biomed. Eng.* **2015**, *8*, 4–16. [CrossRef] [PubMed]
2. Harrison, R.; Watkins, P.; Kier, R.; Lovejoy, R.; Black, D.; Normann, R.; Solzbacher, F. A Low-Power Integrated Circuit for a Wireless 100-Electrode Neural Recording System. *Dig. Tech. Pap.—IEEE Int. Solid-State Circuits Conf.* **2006**, *42*, 123–133. [CrossRef]
3. Sodagar, A.M.; Perlin, G.E.; Yao, Y.; Najafi, K.; Wise, K.D. An Implantable 64-Channel Wireless Microsystem for Single-Unit Neural Recording. *IEEE J. Solid-State Circuits* **2009**, *44*, 2591–2604. [CrossRef]
4. Chi, B.; Yao, J.; Han, S.; Xie, X.; Li, G.; Wang, Z. Low-Power Transceiver Analog Front-End Circuits for Bidirectional High Data Rate Wireless Telemetry in Medical Endoscopy Applications. *IEEE Trans. Biomed. Eng.* **2007**, *54*, 1291–1299. [CrossRef] [PubMed]
5. Chaimanonart, N.; Young, D.J. A Wireless Batteryless in Vivo EKG and Body Temperature Sensing Microsystem with Adaptive RF Powering for Genetically Engineered Mice Monitoring. In Proceedings of the International Solid-State Sensors Actuators and Microsystems Conference, Denver, CO, USA, 21–25 June 2009; pp. 1473–1476. [CrossRef]
6. Zhao, J.; Ghannam, R.; Htet, K.O.; Liu, Y.; Law, M.-K.; Roy, V.A.L.; Michel, B. Self-Powered Implantable Medical Devices Photovoltaic Energy Harvesting Review. *Adv. Healthc. Mater.* **2020**, *9*, 2000779. [CrossRef]
7. Kiourti, A.; Nikita, K.S. A Review of Implantable Patch Antennas for Biomedical Telemetry: Challenges and Solutions. *IEEE Antennas Propag. Mag.* **2012**, *54*, 210–228. [CrossRef]
8. Bhamra, H.; Huang, Y.W.; Yuan, Q.; Irazoqui, P. An Ultra-Low Power 2.4 GHz Transmitter for Energy Harvested Wireless Sensor Nodes and Biomedical Devices. *IEEE Trans. Circuits Syst. II Express Briefs* **2021**, *68*, 206–210. [CrossRef]
9. Afroz, S.; Thomas, S.W.; Mumcu, G.; Saddow, S.E. Implantable SiC based RF antenna biosensor for continuous glucose mon-itoring. In Proceedings of the SENSORS, 2013 IEEE, Baltimore, MD, USA, 3–6 November 2013; pp. 1–4. [CrossRef]
10. Sun, Y.; Greet, B.; Burkland, D.; John, M.; Razavi, M.; Babakhani, A. Wirelessly powered implantable pacemaker with on-chip antenna. In Proceedings of the 2017 IEEE MTT-S International Microwave Symposium (IMS), Honolulu, HI, USA, 4–9 June 2017; pp. 1242–1244. [CrossRef]
11. Chung, W.Y.; Le, G.T.; Tran, T.V.; Nguyen, N.H. Novel Proximal Fish Freshness Monitoring Using Batteryless Smart Sensor Tag. *Sens. Actuators B Chem.* **2017**, *248*, 910–916. [CrossRef]
12. Gilmore, C.; Mojabi, P.; Zakaria, A.; Ostadrahimi, M.; Kaye, C.; Noghanian, S.; Shafai, L.; Pistorius, S.; Lovetri, J. A Wideband Microwave Tomography System with a Novel Frequency Selection Procedure. *IEEE Trans. Biomed. Eng.* **2010**, *57*, 894–904. [CrossRef]
13. Mikhelson, I.V.; Bakhtiari, S.; Elmer, T.W.; Sahakian, A.V. Remote Sensing of Heart Rate and Patterns of Respiration on a Stationary Subject Using 94-GHz Millimeter-Wave Interferometry. *IEEE Trans. Biomed. Eng.* **2011**, *58*, 1671–1677. [CrossRef]
14. Dilello, A.T.; Byun, G.S. An ultra-low power ASK modulator for back telemetry applications. In Proceedings of the IEEE WAMICON 2013, Orlando, FL, USA, 7–9 April 2013; pp. 1–4. [CrossRef]
15. Kiourti, A.; Nikita, K.S. Miniature Scalp-Implantable Antennas for Telemetry in the MICS and ISM Bands: Design, Safety Considerations and Link Budget Analysis. *IEEE Trans. Antennas Propag.* **2012**, *60*, 3568–3575. [CrossRef]
16. Kim, J.; Rahmat-Samii, Y. Implanted Antennas inside a Human Body: Simulations, Designs, and Characterizations. *IEEE Trans. Microw. Theory Tech.* **2004**, *52*, 1934–1943. [CrossRef]
17. Song, L.; Rahmat-Samii, Y. An End-to-End Implanted Brain-Machine Interface Antenna System Performance Characterizations and Development. *IEEE Trans. Antennas Propag.* **2017**, *65*, 3399–3408. [CrossRef]
18. Naqvi, S.A.R.; Mobashsher, A.T.; Mohammed, B.; Foong, D.; Abbosh, A. Benign and Malignant Skin Lesions: Dielectric Characterization, Modelling and Analysis in Frequency Band 1 to 14 GHz. *IEEE Trans. Biomed. Eng.* **2022**, 1–12. [CrossRef] [PubMed]
19. Elshaekh, D.; Kayed, S.; Shawkey, H. Single-Chip Two Antennas for Mm-Wave Self-Powering and Implantable Biomedical Devices. *Appl. Comput. Electromagn. Soc. J.* **2021**, *36*, 885–893. [CrossRef]
20. Zhang, Y.; Liu, C.; Liu, X.; Zhang, K.; Yang, X. A Wideband Circularly Polarized Implantable Antenna for 915 MHz ISM-Band Biotelemetry Devices. *IEEE Antennas Wirel. Propag. Lett.* **2018**, *17*, 1473–1477. [CrossRef]
21. Faisal, F.; Zada, M.; Ejaz, A.; Amin, Y.; Ullah, S.; Yoo, H. A Miniaturized Dual-Band Implantable Antenna System for Medical Applications. *IEEE Trans. Antennas Propag.* **2020**, *68*, 1161–1165. [CrossRef]
22. Xia, Z.; Li, H.; Lee, Z.; Xiao, S.; Shao, W.; Ding, X.; Yang, X. A Wideband Circularly Polarized Implantable Patch Antenna for ISM Band Biomedical Applications. *IEEE Trans. Antennas Propag.* **2020**, *68*, 2399–2404. [CrossRef]
23. Green, R.B.; Hays, M.; Mangino, M.; Topsakal, E. An Anatomical Model for the Simulation and Development of Subcutaneous Implantable Wireless Devices. *IEEE Trans. Antennas Propag.* **2020**, *68*, 7170–7178. [CrossRef]
24. Zada, M.; Shah, I.A.; Basir, A.; Yoo, H. Ultra-Compact Implantable Antenna with Enhanced Performance for Leadless Cardiac Pacemaker System. *IEEE Trans. Antennas Propag.* **2021**, *69*, 1152–1157. [CrossRef]
25. Blauert, J.; Member, S.; Kang, Y.; Kiourti, A. In Vivo Testing of a Miniature 2.4/4.8 GHz Implantable Antenna in Postmortem Human Subject. *IEEE Antennas Wirel. Propag. Lett.* **2018**, *17*, 2334–2338. [CrossRef]
26. Byun, G.S.; Kim, Y.; Kim, J.; Tam, S.W.; Chang, M.C.F. An Energy-Efficient and High-Speed Mobile Memory I/O Interface Using Simultaneous Bi-Directional Dual (Base+RF)-Band Signaling. *IEEE J. Solid-State Circuits* **2012**, *47*, 117–130. [CrossRef]
27. Gao, Y.; Zheng, Y.; Diao, S.; Da Toh, W.; Ang, C.W.; Je, M.; Heng, C.H. Low-Power Ultrawideband Wireless Telemetry Transceiver for Medical Sensor Applications. *IEEE Trans. Biomed. Eng.* **2011**, *58*, 768–772. [CrossRef] [PubMed]

28. Lee, S.Y.; Cheng, P.H.; Tsou, C.F.; Lin, C.C.; Shieh, G.S. A 2.4 GHz ISM Band OOK Transceiver with High Energy Efficiency for Biomedical Implantable Applications. *IEEE Trans. Biomed. Circuits Syst.* **2020**, *14*, 113–124. [CrossRef] [PubMed]
29. Gabriel, C.; Gabriel, S.; Corthout, E. The Dielectric Properties of Biological Tissues: I. Literature Survey. *Phys. Med. Biol.* **1996**, *41*, 2231–2249. [CrossRef]
30. Ture, K.; Devos, A.; Maloberti, F.; Dehollain, C. Area and Power Efficient Ultra-Wideband Transmitter Based on Active Inductor. *IEEE Trans. Circuits Syst. II Express Briefs* **2018**, *65*, 1325–1329. [CrossRef]
31. Gusland, D.; Christiansen, J.M.; Torvik, B.; Gurbuz, S.Z.; Fioranelli, F.; Ritchie, M. Open Radar Initiative: Large Scale Dataset for Benchmarking of Micro-Doppler Recognition Algorithms. In Proceedings of the 2021 IEEE Radar Conference (RadarConf21), Atlanta, GA, USA, 7–14 May 2021.
32. Lin, Y.; Park, S.; Chen, X.; Wentzloff, D.; Yoon, E. 4.32-PJ/b, Overlap-Free, Feedforward Edge-Combiner-Based Ultra-Wideband Transmitter for High-Channel-Count Neural Recording. *IEEE Microw. Wirel. Components Lett.* **2018**, *28*, 52–54. [CrossRef]
33. Zhang, Z.; Li, Y.; Mouthaan, K.; Lian, Y. A Miniature Mode Reconfigurable Inductorless IR-UWB Transmitter-Receiver for Wireless Short-Range Communication and Vital-Sign Sensing. *IEEE J. Emerg. Sel. Top. Circuits Syst.* **2018**, *8*, 294–305. [CrossRef]
34. Byeon, C.W.; Eun, K.C.; Park, C. A 2.65-PJ Bit 12.5-Gbs 60-GHz OOK CMOS Transmitter and Receiver for Proximity Communications. *Medium* **2020**, *68*, 1–6. [CrossRef]
35. De Streel, G.; Stas, F.; Gurne, T.; Durant, F.; Frenkel, C.; Cathelin, A.; Bol, D. SleepTalker: A ULV 802.15.4a IR-UWB Transmitter SoC in 28-Nm FDSOI Achieving 14 PJ/b at 27 Mb/s with Channel Selection Based on Adaptive FBB and Digitally Programmable Pulse Shaping. *IEEE J. Solid-State Circuits* **2017**, *52*, 1163–1177. [CrossRef]